REPORT DOCUMENTATION PAGE

Form Approved
OMB No. 0704-0188

1. REPORT DATE *(DD-MM-YYYY)*	2. REPORT TYPE	3. DATES COVERED *(From - To)*
05-26-2004	Final Technical Report	06-01-1998 to 05-26-2004

4. TITLE AND SUBTITLE
Investigation of Subcritical Fatigue Crack Growth in Gamma Titanium Aluminides

5a. CONTRACT NUMBER
N00014-98-1-0390 ADMIN. MOD. # P00007

5b. GRANT NUMBER

5c. PROGRAM ELEMENT NUMBER

6. AUTHOR(S)
Blair London

5d. PROJECT NUMBER
PR #: 00PR01786-01

5e. TASK NUMBER

5f. WORK UNIT NUMBER

7. PERFORMING ORGANIZATION NAME(S) AND ADDRESS(ES)
California Polytechnic State University
College of Engineering
Materials Engineering
San Luis Obispo, CA 93407

8. PERFORMING ORGANIZATION REPORT NUMBER
GDO 98-102

9. SPONSORING/MONITORING AGENCY NAME(S) AND ADDRESS(ES)
California Polytechnic State University Foundation
Sponsored Programs Department
Foundation Administration Bldg. 15
San Luis Obispo, CA 93407

10. SPONSOR/MONITOR'S ACRONYM(S)
CPSU Foundation

11. SPONSOR/MONITOR'S REPORT NUMBER(S)
53630

12. DISTRIBUTION/AVAILABILITY STATEMENT
APPROVED FOR PUBLIC RELEASE - DISTRIBUTION UNLIMITED

13. SUPPLEMENTARY NOTES
CFDA: 12.300 DUNS #: 008963233 CAGE: 4B563

14. ABSTRACT
Our titanium aluminide alloy was readily heat treated to a fully lamellar state by holding at 1345C for 1.5 hours and furnace cooling resulting in a grain size of 330 muon m. The yield stress, ultimate stress, and total elongation were 315MPa, 465MPa, and 0.46% respectively. The fully lamellar microstructure shows significant work hardening. No long cracks initiated at R=0.1 and variation max=300MPa with up to 1.4 million cycles.

15. SUBJECT TERMS
Titanium aluminides, fully lamellar microstructure

16. SECURITY CLASSIFICATION OF:			17. LIMITATION OF ABSTRACT	18. NUMBER OF PAGES	19a. NAME OF RESPONSIBLE PERSON
a. REPORT	b. ABSTRACT	c. THIS PAGE			Blair London
Public Release	SAR	SAR	SAR	18	19b. TELEPHONE NUMBER *(Include area code)* (805) 756-2536

CHAPTER 1

Introduction to TiAl Basics

Titanium aluminides (TiAl) have been investigated for possible application as high-temperature structural materials for many years. The interest is due mainly to their low mass compared to nickel aluminides or nickel based superalloys. They have theoretically good high-temperature strengths and ductilities, however much research has been focused on improving their low- to room-temperature properties. Several variations of TiAl, including fully lamellar, dual phase, and triple phase intermetallics exist. The fully lamellar, known as γ-TiAl, consists of alternating plates of $L1_0$(TiAl) and DO_{19}(Ti_3Al) phases. The double phase includes grains of α_2 D019 and the triple phase includes a B2 phase. This project investigated the fatigue properties of the fully lamellar microstructure.

Gamma TiAl can be processed by several different methods, including hot-rolling. The material is then heat treated to produce the desired microstructure. Gamma TiAl compostitions typically contain 46-54(atomic %)Al, and 1-10(atomic %)(V, Cr, Mn, W, Mo, Nb, Ta).1 At more or less than the stoichiometric ratio, Ti and Al atoms will substitute for one another in the $L1_0$ lattices.2 The bonding relationships of TiAl are only generally understood, but progress has been made in developing the binary phase diagram in the 30-60 atomic percent Al regions, and this is shown in Figure 1.3

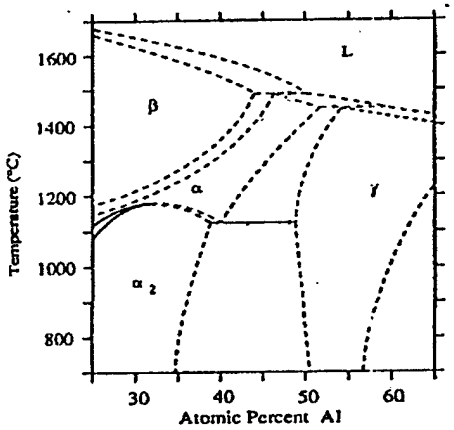

Figure 1 Central portion of TiAl phase diagram.

The family of titanium aluminides known as gamma TiAl can have varying microstructures according to how the material was processed. Through different temperatures, saturation times, and various cooling rates, large differences in microstructures can be obtained. Always present in this family of TiAl are gamma grains which have the aforementioned alternating plates. The duplex microstructure is obtained by using lower heat treatment temperatures and/or saturation times than would be used for a fully lamellar microstructure. This results in a microstructure consisting of α_2 ($D0_{19}$ phase) and lamellar colonies. To obtain the fully lamellar microstructure, the material must be heat treated above its alpha transus temperature. The lamellar colony size may be modified by saturating the material above the alpha transus for durations between one and four hours, which results in colony sizes of 75-600μm.

To understand the effects of alloy content upon mechanical properties, the nature of bonding in the material should be understood. This has been a subject of much investigation. For increases in Al content over stoichiometric the $L1_0$ phase, shown in Figure 2, will have less metallic bonding, with a more covalent nature.

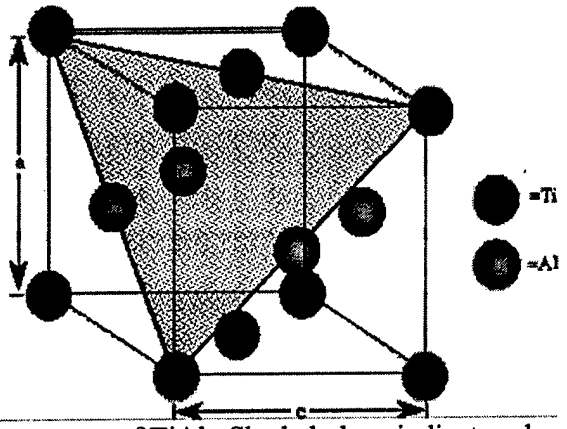

Figure 2 The $L1_0$ structure of TiAl. Shaded plane indicates close-packed plane of alternating Ti and Al rows.

This is evident in the increase in c/a ratio from 1.02 to 1.03 for increasing Al contents. Al atoms which substitute for Ti on the corners or upper and lower faces will decrease the

a axis due to lesser bond lengths for more bonds with a higher covalent nature. It has been shown that the 0.2% flow stress decreases for increased Al contents by a small degree, which is consistent with the small change in c/a ratio.4 The strain to failure is also greatly affected by the alloy content, with the highest values having been found for Ti-48Al.5 The effects of adding other elements can affect both the elongation to failure (ε_f) and c/a ratio, and these are shown in Figure 3.6

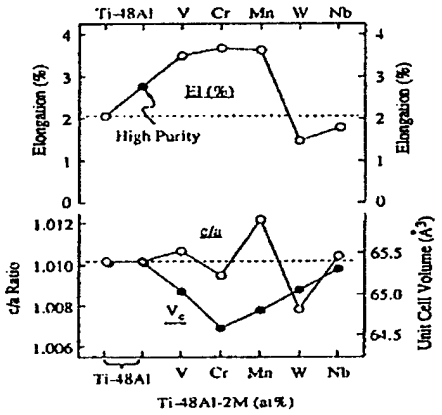

Figure 3 Effects of transition metal alloying in Ti-48Al.

It is assumed that transition elements will preferentially substitute for Ti atoms since their sizes and valence shells are most similar. How these factors contribute to the deformation mechanics has been investigated to a lesser degree.

It is necessary in predicting the behavior of TiAl to understand the complicated nature of dislocation motion. Both ordinary and superdislocations are present in the $L1_0$ phase. There are large densities of ½<110] ordinary dislocations and some <011] superdislocations.7 The motion of the ordinary dislocations controls the deformation at low temperatures. From room temperature to approximately 600C the ductility of TiAl goes down while its yield stress increases.8 This is explained by the fact that the superdislocations are increasingly able to move, which allows them to dissociate as shown for a perfect screw:9

$$<01] \rightarrow \frac{1}{6}[11\bar{2}] + SISF + \frac{1}{6}[\bar{1}\bar{1}2] \qquad \text{Eq. 1}$$
$$+ APB + \frac{1}{6}[\bar{1}\bar{1}\bar{2}] + SISF + \frac{1}{6}[\bar{1}12]$$

The SISF term refers to superlattice intrinsic stacking factor, and APB refers to antiphase boundaries. This dissociation results in a locking configuration which causes the ordinary dislocations to be pinned by the supers, causing low strain to failure (ε_f) values for TiAl at room temperature. Further increasing temperature will allow the supers to move enough to remove the Shockley partials allowing for more deformation. The movement of dislocations is important not only for understanding the yield and strain behavior, it is an important factor in the initiation and propagation of fatigue cracks through dislocation pileups. These pileups can cause cracks by forming slip bands, forming cracks in grain boundaries, and by dislocation transmission into the DO_{19} phase. These effects are more investigated in a following section on modeling.

Short Cracks

The growth of fatigue cracks has been extensively studied, and for cracks which are "long" the propagation theory is well understood. Most of the approaches are based on linear elastic fracture mechanics (LEFM) typified by Equation 2,

$$\frac{da}{dN} = A(\Delta K)^n \qquad \text{Eq. 2}$$

where da/dN is crack advance per cycle, A and n are empirically determined constants, and ΔK is the range of stress intensity factor. Figure 4 shows a typical plot of how a crack proceeds according to LEFM predictions.

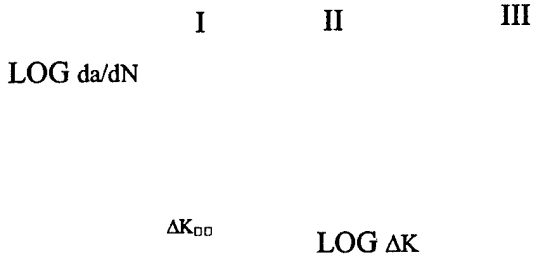

Figure 4 Plot of log crack growth per cycle versus log of stress intensity factor range due to propagating crack. The threshold value of stress intensity (ΔK_{TH}) is the value below which cracks are assumed to not grow.

Short cracks have various complicating factors, which include the inability of LEFM to deal with cracks shorter that ~0.5mm, the three dimensional nature of short cracks, and metallographic features tend to play large roles for small cracks.[10] Irwin showed that if the plastic zone ahead of a crack tip is less than 1/50 the size of the crack, that LEFM is sufficiently accurate.[11] In a material which shows a large degree of cyclic hardening such as TiAl[12], LEFM will predict much slower crack propagation rates than would be observed. The more common approach to modeling short cracks is to use elastic-plastic fracture mechanics (EPFM). The basic form of EPFM equations is shown in Equation 3,

$$\frac{da}{dN} = A(\Delta\varepsilon_p)^n a \qquad \text{Eq. 3}$$

where $\Delta\varepsilon_p$ is the reversed plastic strain range, and A and n are empirically determined for use in EPFM analyses. $\Delta\varepsilon_p$ may be reduced by cyclic hardening or by the transition from plane stress to plane strain in the interior of a sample. Short cracks will start out with a rate proportional to their own length per cycle, then decelerate as they approach the curve described by LEFM, assuming no other discontinuities impede or accelerate their progress.

The manner by which the crack initiates is very important since its size and orientation will greatly affect whether or not it will propagate. Once a sufficient size is achieved and it becomes a long crack, it will dominate the other short cracks which will become non-propagating. This assumes short cracks will not link up with the main crack or the main crack is arrested. The initiation will occur by favorably inclined slip systems, grain boundaries, or at surface defects such as machining scratches.

Modeling Theory

Understanding short crack phenomena in intermetallics such as titanium aluminides (TiAl) is difficult and must be approached from several directions at once. First, an empirical knowledge of the mechanical behavior of intermetallic materials is required. This is not a trivial proposition since the behavior of intermetallic materials varies widely with only small changes in composition, environment, and/or processing. This limits the effectiveness of an experimentalist approach for developing a material.

To approach real understanding requires first principle (ab initio) techniques, or techniques which assume as little information as is practically possible. There are two fundamental levels of first principle analysis: qualitative and quantitative. Qualitative analysis is the first step, and is usually the last in many cases, for predicting the behavior of a material. However the difficulty in understanding the nature of bonding in intermetallics requires a deeper method. Quantitative analysis incorporates both empirical test data, and qualitative descriptions into its more universal utility.

Before an attempt is made to understand and predict the mechanical properties, analysis of the basic facts is necessary. The behavior of dislocations, superdislocations, and twins have been well-investigated, and so are an opportune place to begin. The first clue about the nature of γ-TiAl is the rise in yield stress as temperature goes up. Intuitively this is odd, since it should become easier to move dislocations, both ordinary and super, with increasing temperature. The toughness of dual-phase($L1_0/DO_{19}$) and triple-phase($L1_0/DO_{19}/B_2$) γ-TiAl is odd. None of the constituents are particularly tough, so it seems unclear why a combination should be tough. The individual phases show very little plasticity or other toughening mechanisms. It has been shown that the $L1_0$ phase shows fairly high densities of ordinary dislocations of type ½<100], yet this phase alone shows only small toughness.13 Further complicating the analysis, additions of Nb, V, and increasing Al concentrations above stoichiometric values in the $L1_0$ phase tend to increase the c/a ratio of the $L1_0$ phase and reduce ductility.14 These are not necessarily related effects, since the c/a ratio change is quite small. These facts are a background against which some analysis may be cast.

Heavy qualitative analysis has been performed on the gathered evidence. Again, basic scientific knowledge is the foundation upon which to build. Ti and Al will bond metallically and covalently. The greater strength of covalent bonds will pull the cationic centers closer together. This will result in d-shell orbital splitting in the Ti valence electrons, and possibly stabilize hybrid sp-shells in the Al electrons. In any case, it is clear from the crystal structure shown in Figure 2 why deviation from stoichiometric compositions will change the overall unit cell c/a ratio. The close-packed planes of the $L1_0$ structure will be less densely packed since they consist of alternating rows of Ti and

Al inner cores. This explanation lends itself to describing the effects of other elements. Those which localize bonding in the planes will reduce the c/a ratio, and those which do not will increase it. This could be an excellent way of quickly determining the nature of the bonding, more metallic will increase c/a and more covalent will decrease it. This is not only applicable to aspect ratio, since in ordered intermetallics such as TiAl, anti-phase boundary (APB) energies will be effected by the nature of the passing superdislocation. More or less Al atom substitutions with the lattice will lower the APB energy. It is unclear which concentration deviation will have the lower energy, but it seems that more Al ions would be less in energy than more Ti ions, since Al-Al interactions will have less energy (more metallic) than Ti-Ti interactions. Additionally, surface energies will be dramatically affected by the bonding of the material. It has been shown that microcrack nucleation is likely the determining factor in short crack propagation.15 Determination of when microcracks will nucleate, and which will propagate has for the most part eluded researchers using standard (and non-standard) continuum mechanics methods. The surface energies of each cleavage plane, grain-boundary interfaces, and twin boundaries have to be evaluated. Once environmental and compositional effects are brought in, it is too difficult to simply test. Increased bond localization will tend to increase the energy to create a new surface. Therefore it would be useful to model the electron distributions in TiAl. A model for microcrack nucleation is presented in the next section. It seems that an understanding of where electrons are is very important to the mechanical properties of TiAl, or any material for that matter. Not for calculations sake, but to refine our understanding of how the mechanisms are cooperating and competing.

Quantitative analysis of materials has recently become very fashionable and feasible with the availability of high-power computing resources. Various "tight-binding" methods have been used. In simple terms, these methods allow for the calculations of the interatomic potentials. Common features of the various methods are approximations of valence shell interactions, large numbers of atoms, numerical (non-analytic) solutions, and recursive determination of various fitting parameters. Using some established values, usually the elastic constants (C_{11}, C_{12}, C_{44}), the numerical

models are adjusted until the model becomes "self-consistent." This is the point where large numbers of fitting values can be combined with the same order of accuracy. These methods are computationally intense, requiring significant computing power and/or programming ability. Appendix I involves determining the angular dependence of microcrack nucleation on burgers vector, direction of travel, and interface characteristics using Mathematica. This model was developed by Yoo for TiAl specifically.16 It is easily incorporated into a more complete tight-binding model.

Microcrack Nucleation

One mechanism by which microcracks may be nucleated is by dislocation pileups at an interface such as grain or twin boundaries. Ideally these boundaries would be sources and sinks for dislocations or at least initiate deformation in an adjacent grain. In these cases, $\Delta\varepsilon_p$ would be reduced slowing propagating cracks or just not forming them at all. However, microcrack nucleation within the grain or along grain boundaries can occur. Yoo determined the critical stress concentration (τ_c) required to initiate these cracks with dislocation pileups shown in Equation 4,

where K is an energy factor, $\tau_c = \frac{Kb}{2\pi l}^{1/2} \frac{\Gamma}{H(\theta)}^{1/2}$ b is the [ ]tude of the burgers vector, l is the length of the dislocation pileup, and Γ is the surface energy of the created surface. The term $H(\theta)$ is the angular dependence on the motion of mixed dislocations. Equation 5 shows $H(\theta)$,

$$H(\theta) = \sigma_e f_I(\theta) + \sigma_e f_{II}(\theta) + \sigma_s f_{III}(\theta) \quad \text{Eq. 5}$$

where $\rho_e = K_e \sin^2\beta/K$, $\rho_s = K_s \sin\beta/K$, β is the angle between the burgers vector and dislocation line direction indicating the mixity of dislocation modes, and the subscripts e and s indicate edge and screw dislocations respectively. The f terms represent the angular functions of elastic stress fields ahead of a crack tip. Using the program in Appendix I, resulted in Figure 5 angular dependence of stress for dislocations of varying nature. The figure clearly shows that the type of dislocation will matter in the nucleation of microcracks. This may be an important clue as to why lamellar plate thicknesses matter in the nucleation of microcracks within

gamma grains.

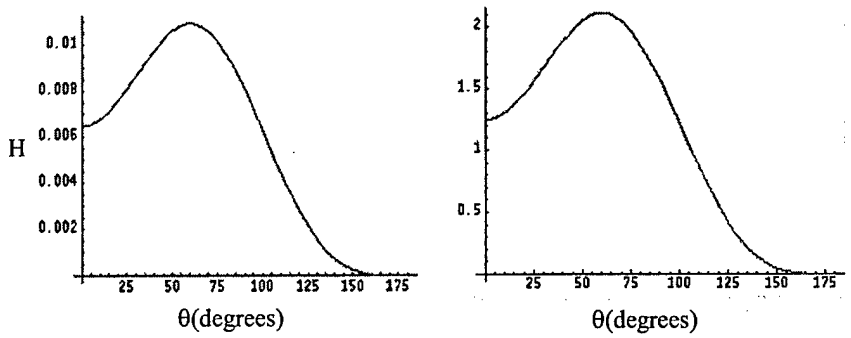

Figure 5 Graphs of angular stress dependence of mixed-mode ½<110] dislocations at a (111) twin boundary. (a) shows graph for β=15°, and (b) shows graph for β=75° for a farfield stress consisting only of σ_{yy}.

Two-center Approximation

A very complete method for calculating the total energy of a material was developed by Papaconstantopoulus and Mehl17 for PdH systems. They modeled the material using energy band solutions for s, p, and d orbitals. Solving the Hamiltonian for A-B interactions requires 14 two-center parameters $P_i(r)$ utilizing a polynomial incorporating center to center differences, as shown in Equation 6.

$$P_i = a_i + b_i r + c_i r^2 \quad \text{Eq. 6}$$

For this equation all the iterated coefficients in the polynomial are fitting parameters, as is λ. A "cutoff" function f(r) is used to limit the calculations to a given number (usually 5 for transition metals and Lanthanide's of valence shells. More than this would not be useful as Slater's rules for nuclear shielding show that the outer shell electrons are fairly independent of nuclear effects.18 Further calculations of volume effects in a tight-binding model are useful, but are not included or instructive for this discussion. The benefit of this method over other two-center approximations is that it does not rely on pair-potentials for fitting the total energy. Pair-potential methods, typified by the Lennard-Jones approach, are computationally costly

and so require more computing power, longer calculation times, and/or less numbers of atoms within a given model. Ultimately this method requires only a 14x14 matrix for each atom in the model assuming only A-A and A-B interactions. This model cannot incorporate environmental effects, and it would seem to be very difficult to incorporate vacancies and other absentee defects.

Tight-Binding Model with Modified Two-Center Approximations

As discussed in the previous section, the two-center approximation for tight-binding has some fundamental difficulties dealing with environmental effects, and certainly non-localized bonding as in metallic bonding would be ill-represented. Wang, et. al., have developed a method which incorporates conditional tight-binding constant and repulsive potentials.19 Essentially this model extends the two-center approximations by incorporating the effects of higher coordination numbers and shielding by the next nearest neighbors by nearest neighbors. Basic crystal field theory indicates that as coordination numbers increase, more electron-electron repulsion's occur, weakening the bonds between the atom and its first nearest neighbors. Wang, et. al., modeled bonding between carbon and silicon based upon Equation 7,

$$V(r_{ij}) = R_{ij}^{\alpha} e^{\beta R_{ij}^{\gamma}} S_{ij} \qquad \text{Eq. 7}$$

where $V(r_{ij})$ represents the solutions for each of the bond interactions; σ-type bonds between sp, ss, and pp orbitals, and the π-type bonds between pp orbitals. Recall that both C and Si form sp^3-hybrids and result in those four types of bonds. The α's are fitting parameters which may or may not change for different types of bonding. R_{ij} and S_{ij} are scaling (normalized distances) and screening functions, respectively. The scaling function is determined by Equation 8,

$$S_{ij} = \tanh(\alpha(1)\exp(\beta(r_{il}+r_{jl}-r_{ij}))) \qquad \text{Eq. 8}$$

where the β's are sc parameters. Eventually calculations of R_{ij} and other values lead to a model which can become self-consistent for calculating energy bands. This model resulted in excellent reproduction of

calculated energy bands, structure types (bcc vs fcc vs diamond cubic vs others), and elastic constants. This approach is likely the best two-center model for the mixed bonding environment for TiAl. A similar method developed by Panova was used to model dislocation cores in the $L1_0$ structure.20 It was shown that the anomalous hardening of TiAl with increasing temperature was likely due to <001] and <110] superdislocations becoming glissile with increased temperature. Eventually, these dislocations form Shockley partials which form locking configurations. These locking configurations formed stacking faults of which Superlatttice Intrinsic Stacking Faults (SISF) played a major role. In this case computational modeling was able to effectively propose and/or confirm a behavior whose explanation had been elusive to experimentalists.

Embedded Atom Methods

Two-center approximations, however, have fallen out of favor due to the large amount of assumptions and patches need for accuracy in a mixed and non-localized bonding environment. Many body methods have shown themselves to be superior even though less a priori data is used for their interatomic potentials. These many body methods use the pair potential energy model along with an additional "embedding" function, hence they are known as embedded atom methods (EAM). A typical total energy equation is shown in Equation 9.

The pair potential is $V(r_{ij})$ $E_{tot} = \frac{1}{2}\sum_{ij} V(r_{ij}) + \sum_{i} F(\rho_i)$ and the Eq. 9 ding energy is F which is a function of the effects of the other atoms at site i, represented in Equation 10.

The function $\rho(r_{ij})$ is the atomic $\rho_i = \sum_{j \neq i} \rho(r_{ij})$ Eq. 10 density functi[illegible] material. This is the basis upon which most current methods of modeling materials are being based. There is much contention about how the embedding function should be developed, and the specifics are beyond the scope of this report.

CHAPTER 2

Procedure

To determine the crack initiation and short crack propagation rates in the fully lamellar γ-TiAl required many preparatory stages. The material had to be heat treated appropriately, its lamellar colony size quantified, and its monotonic stress-strain behavior determined. Only then could the fatigue behavior be investigated.

The TiAl obtained for this investigation was hot forged creating a dual-phase microstructure as shown in Figure 6.

Figure 6 Dual phase microstructure of forged TiAl, 400X etched with Kroll's Reagent.

To develop a fully lamellar microstructure, the material was heat treated at 1345C for 1.5 hours then furnace cooled. The resulting microstructure is shown in Figure 7.

Figure 7 Fully lamellar microstructure of heat treated TiAl, 100X etched with Kroll's

Reagent.

To obtain both grain size and distribution, a Buehler Image Analyzer was used. Three samples from randomly selected sections of the heat treated forging were selected for analysis. Eight fields from each sample were imaged and analyzed. To determine the consistency of the process, the colony size results were tested using statistical process control (SPC) methods. After heat treatment, xray diffraction (XRD) was performed using a Siemens Model 5000 Diffraktometer to determine whether or not the material consisted only of lamellar grains with no B2 phase, and whether TiB_2 was present.

To select an appropriate stress range for fatigue testing, the yield stress, ultimate stress, and ultimate elongation was determined. Two stress-strain tests were conducted on the circular gage section samples to be used for fatigue testing, shown in Figure 8.

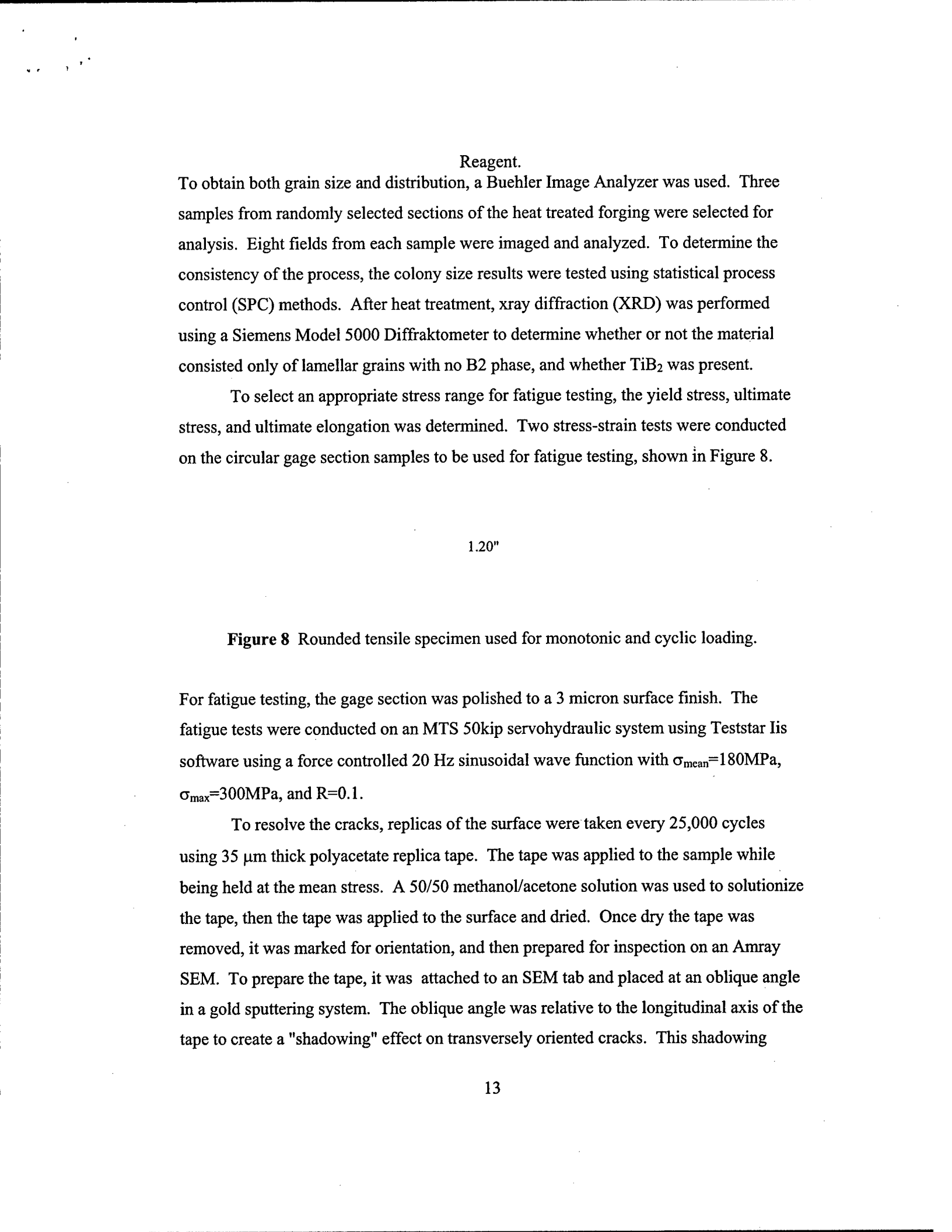

Figure 8 Rounded tensile specimen used for monotonic and cyclic loading.

For fatigue testing, the gage section was polished to a 3 micron surface finish. The fatigue tests were conducted on an MTS 50kip servohydraulic system using Teststar Iis software using a force controlled 20 Hz sinusoidal wave function with σ_{mean}=180MPa, σ_{max}=300MPa, and R=0.1.

To resolve the cracks, replicas of the surface were taken every 25,000 cycles using 35 μm thick polyacetate replica tape. The tape was applied to the sample while being held at the mean stress. A 50/50 methanol/acetone solution was used to solutionize the tape, then the tape was applied to the surface and dried. Once dry the tape was removed, it was marked for orientation, and then prepared for inspection on an Amray SEM. To prepare the tape, it was attached to an SEM tab and placed at an oblique angle in a gold sputtering system. The oblique angle was relative to the longitudinal axis of the tape to create a "shadowing" effect on transversely oriented cracks. This shadowing

effect was intended to increase the contrast of the cracks.

CHAPTER 3

Results

The colony sizes and distributions were found to be statistically in-control and consistent with more established ASTM E112 grain size methods. The average grain size was determined to be ASTM grain size number 1.69 (~330μm) and the distribution is shown in Figure 9.

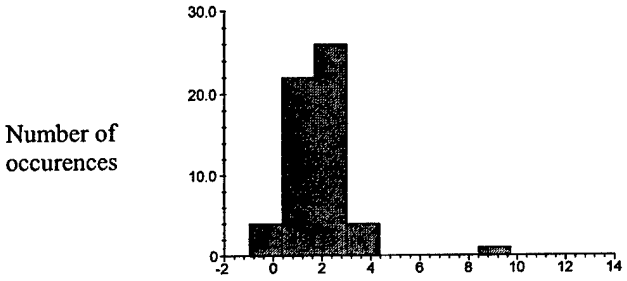

Figure 9 Typical colony size distribution of heat treated TiAl samples.

The distribution of colony size is important since one definition of a short crack is that of a crack which is smaller than the present metallographic features.

The XRD investigation indicated that the only phases present were $L1_0$ and DO_{19}. Figure 10 shows the scan performed on a slab sample of the heat-treated TiAl.

Figure 10 XRD scan of TiAl showing resulting peaks. Scan was performed with step size of 0.10C ...as removed.

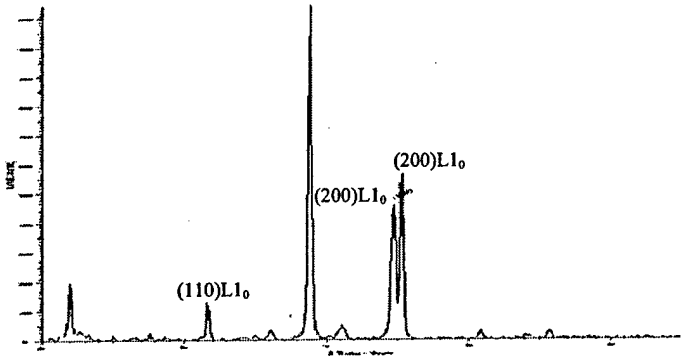

The results of tensile testing are shown in Table I and Figure 11.

Table I Mechanical Properties of fully lamellar TiAl specimens.

	σ_y(MPa)	σ_{UTS}(MPa)	*Total Elongataion*
Sample 1	315	490	0.52
Sample 2	315	440	0.4

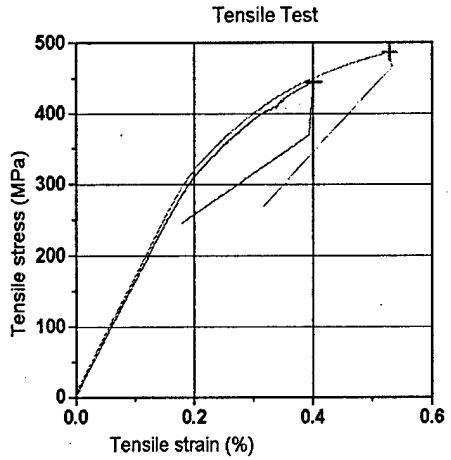

Figure 11 Stress-strain curves for fully lamellar samples.

Significant work hardening is evident in the curves, so it is likely that cracks which nucleate by slip banding would not proceed due to the $\Delta\varepsilon_p$ being reduced by plasticity. Therefore small cracks may propagate by grain boundary nucleation or coalescence.

Two fatigue tests were conducted, one until 650,000 cycles and one until 1.4 million cycles. Both were prematurely terminated by machine malfunctions. Replicates performed on these samples showed no evident cracking, and the tuning state of the machine was not changed during the duration of the tests. Therefore it seems likely that no long cracks developed in this period. Information about short cracks is lacking however, since the surfaces of the samples showed only machining marks which may have obscured initiated and growing small cracks.

CHAPTER 4

Conclusions

1. Our titanium aluminide alloy was readily heat treated to a fully lamellar state by holding at 1345C for 1.5 hours and furnace cooling resulting in a grain size of 330μm.
2. The yield stress, ultimate stress, and total elongation were 315MPa, 465MPa, and 0.46% respectively.
3. The fully lamellar microstructure shows significant work hardening.
4. No long cracks initiated at R=0.1 and σ_{max}=300MPa with up to 1.4 million cycles.

APPENDIX A

Mathematica Program for Modeling the Angular

Dependence of Microcrack Nucleation

```
For[i=0, i <= 6, i++, {
        bet =i*15
        Print["Angle b/w burgers vector and disloc. line direction is ", bet,
  "degrees"]
    Ke=95.2
        Ks=59.9
        K=79.4
        b=0.25(2^2+1+1)^0.5;
        surf=2.25;
        (*stress field functions, ie f11=sigma(xx) for mode 1,
  f12 is sigma (yy) for mode 1*)
    f11=Cos[thet*Degree/2](1-Sin[thet*Degree/2]Sin[3thet*Degree/2]);
    f12=Cos[thet*Degree/2](1+Sin[thet*Degree/2]Sin[3thet*Degree/2]);
    f13=Cos[thet*Degree/2]Sin[thet*Degree/2]Cos[3thet*Degree/2];
    f21=-Sin[thet*Degree/2](2+Cos[thet*Degree/2]Cos[3thet*Degree/2]);
    f22=Sin[thet*Degree/2]Cos[thet*Degree/2]Cos[3thet*Degree/2];
    f23=Cos[thet*Degree/2](1-Sin[thet*Degree/2]Sin[3thet*Degree/2]);
    f31=0;
    f32=-Sin[thet*Degree/2];
    f33=Cos[thet*Degree/2];
    rowe=(Ke/K)*(Sin[bet*Degree])^2;
    Print["Edge component is ", rowe]
    rows=(Ks/K)*(Cos[bet*Degree])^2;
    Print["Screw component is ", rows]
    h1=(rowe*f12)^2+(rowe*f22)^2+(rows*f31)^2;
    h2=(rowe*f21)^2+(rowe*f22)^2+(rows*f23)^2;
    h3=(rowe*f31)^2+(rowe*f32)^2+(rows*f33)^2;
    (* tau1=Pi*(K*b/(2Pi))^0.5*(surf/h1)^0.5; *)
    (* tau2=Pi*(K*b/(2Pi))^0.5*(surf/h2); *)
    (* tau3=Pi*(K*b/(2Pi))^0.5*(surf/h3); *)
    (* Plot[tau1, {thet,0,180}] *)
    Plot[{h1},{thet,0,180},
  PlotStyle->{{RGBColor[1,0,0]},{RGBColor[0,1,0]},{RGBColor[0,0,1]},{
    RGBColor[1,0,1]}}]
    }]
```

1Y-W. Kim, *Intermetallic Alloys Based on Gamma Titanium Aluminides*, JOM, July 1989, pp. 24-30. (hereafter Kim)
2Kim.
3Kim.
4E. Kobayashi, K. Shinmoto, et al., *Effect of Deviation from the Stocichiometry on the Lattice Constants and Strength of the $L1_0$ TiAl-X(X=Cr, V or Nb) Alloys at Ambient Temperature,* TMS Proceedings: Gamma Titanium Aluminides(1995), pp. 347-352.
5Kim.
6Kim.
7J. Panova, D. Farkas, TMS Proceedings: Gamma Titanium Aluminides (1995), pp. 331-338. (hereafter Panova)
8Kim.
9Panova.
10K.J. Miller, *The Short Crack Problem*, Fat. Engr. Mater. Str., 1982, vol. 5, p. 223-232. (hereafter Miller)
11Miller, pp. 223-232.
12K.W. Chen, *The Fatigue Resistance of TiAl-based Alloys*, JOM, July 1997, pp. 53-58.
13M.H. Yoo, TMS Proceedings: Gamma Titanium Aluminides(1995), pp. 255-269. (hereafter Yoo)
14Kim.
15Yoo.
16Yoo.
17D.A. Papaconstantopoulos, M.J. Mehl, *Proc. Mater. Res. Sym.*, Vol. 408 (1996), pp. 31-35.
18G.E. Rodgers, Introduction to Coordination, Solid State, and Descriptive Inorganic Chemistry, McGraw-Hill (1994), p. 219.
19C.Z. Wang, M.S. Tang, B. Pan, C.T. Chan, K.M. Ho, *Proc. Mater. Res. Sym.*, Vol. 408 (1996), pp. 37-42.
20Panova.